

Bni1p, a Yeast Formin Linking Cdc42p and the Actin Cytoskeleton During Polarized Morphogenesis

Marie Evangelista, Kelly Blundell, Mark S. Longtine,
Clinton J. Chow, Neil Adames, John R. Pringle,
Matthias Peter, Charles Boone*

The *Saccharomyces cerevisiae* *BNI1* gene product (Bni1p) is a member of the formin family of proteins, which participate in cell polarization, cytokinesis, and vertebrate limb formation. During mating pheromone response, *bni1* mutants showed defects both in polarized morphogenesis and in reorganization of the underlying actin cytoskeleton. In two-hybrid experiments, Bni1p formed complexes with the activated form of the Rho-related guanosine triphosphatase Cdc42p, with actin, and with two actin-associated proteins, profilin and Bud6p (Aip3p). Both Bni1p and Bud6p (like Cdc42p and actin) localized to the tips of mating projections. Bni1p may function as a Cdc42p target that links the pheromone response pathway to the actin cytoskeleton.

In response to an external pheromone cue, *Saccharomyces cerevisiae* cells arrest cell division in the G_1 phase of the cell cycle, increase the expression of mating genes, and form polarized mating projections directed toward the pheromone source (1, 2). These responses are coordinated by a signal transduction cascade initiated by a cell surface receptor coupled to a heterotrimeric guanosine triphosphate (GTP)-binding protein (G protein). The morphological changes depend on reorganization of the underlying actin cytoskeleton. During projection formation, patches of filamentous actin are localized to the tip of the projection, and actin cables align along the projection axis (1, 2). Elucidation of the molecular basis of projection formation should provide a model for the interactions between signaling pathways and the actin cytoskeleton.

Members of the Rho family of guanosine triphosphatase (GTPase) proteins participate in signaling events that cause reorganization of the cortical cytoskeleton and control processes such as cell morphogenesis, motility, and cytokinesis. These proteins cycle between active (GTP-bound) and inactive [guanosine diphosphate (GDP)-bound] forms at rates determined by specific regulatory proteins. In mammalian cells, GTP-bound Rho proteins promote the formation of filopodia, lamellipodia, and focal adhesions with actin stress fibers (3). Yeast cells

have a set of five Rho-related GTPases, Cdc42p, Rho1p, Rho2p, Rho3p, and Rho4p, that coordinate reorganization of the cytoskeleton and cell surface growth (4–6). In particular, Cdc42p localizes to growth sites (7) and is required for asymmetric cell surface expansion during both budding and mating (4, 5). Both yeast Cdc42p and its mammalian homologs regulate actin assembly (3, 8). Little is known about the targets of Cdc42p required for

this regulation, but they are likely to include proteins that either bind actin directly or control the function of actin-binding proteins (3, 8). Here, we present evidence that *S. cerevisiae* Bni1p, a protein implicated in cytokinesis and cell polarization during bud development (9, 10), may link Cdc42p to the actin cytoskeleton during pheromone response.

We isolated two independent mutant alleles of *BNI1* in screens designed to identify genes required for efficient mating (11). Cells containing a *bni1* deletion mutation were nearly normal for pheromone-induced G_1 arrest and expression of a mating gene (*FUS1*) (12). However, under conditions in which the majority of wild-type cells had projections with concentrated cortical actin patches at their tips, *bni1* mutant cells remained depolarized with a round cell shape and randomly distributed actin patches (Fig. 1A). Moreover, Bni1p was concentrated at the growing tips of normal mating projections (Fig. 1C). Thus, Bni1p is not important for cell cycle arrest or transcriptional activation but may be an effector of the pheromone-response pathway involved in polarized morphogenesis.

Bni1p is a member of the formin family of proteins, which also includes the products of the vertebrate *limb deformity* locus, the *Drosophila* genes *diaphanous* and

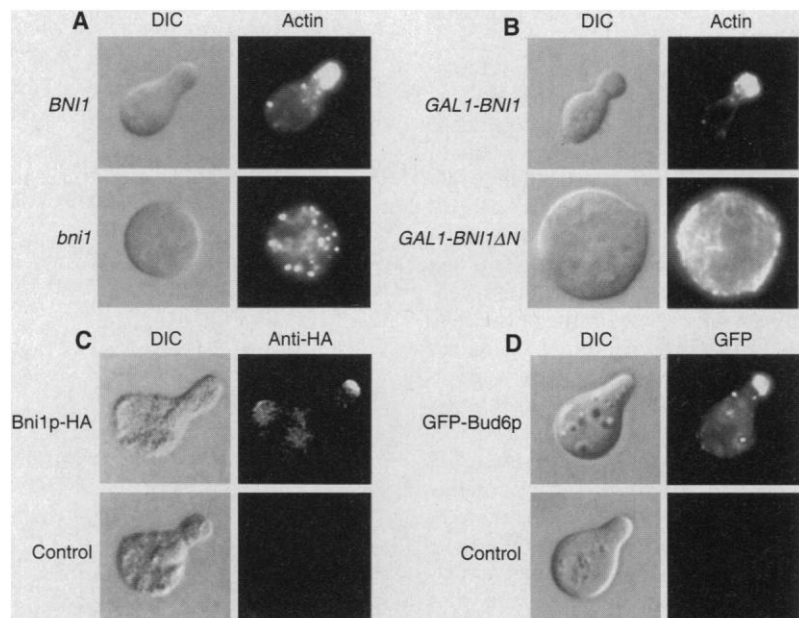


Fig. 1. Involvement of Bni1p in reorganization of the actin cytoskeleton during polarized morphogenesis and localization of Bni1p and Bud6p in mating projections. **(A)** Wild-type (*BNI1*) and *bni1* mutant cells after exposure to pheromone. Cells were visualized by differential interference contrast (DIC) and fluorescence microscopy after staining of actin with rhodamine-phalloidin (14). Final magnifications are the same in each panel. **(B)** Wild-type cells overexpressing *BNI1* or *BNI1ΔN* (14). **(C)** Wild-type cells expressing HA epitope-tagged Bni1p or nontagged Bni1p were exposed to pheromone, then examined by immunofluorescence with monoclonal antibodies to HA (29). **(D)** Wild-type cells expressing GFP-Bud6p and control cells were exposed to pheromone, then observed for a GFP signal (29).

M. Evangelista, K. Blundell, C. J. Chow, N. Adames, C. Boone, Institute of Molecular Biology and Biochemistry, Simon Fraser University, Burnaby, British Columbia V5A 1S6, Canada.

M. S. Longtine and J. R. Pringle, Department of Biology, University of North Carolina, Chapel Hill, NC 27599-3280, USA.

M. Peter, Swiss Institute for Experimental Cancer Research, 1066 Epalinges, Switzerland.

*To whom correspondence should be addressed.

cappuccino, the *Aspergillus nidulans* gene *figA* (*sepA*), and the *Schizosaccharomyces pombe* genes *fus1* and *cdc12* (13). These proteins participate in cytokinesis, the establishment of cell polarity, and vertebrate limb formation. Formins share two regions of sequence similarity, designated FH1 and FH2. The FH1 domain (amino acids 1230 to 1330 in Bni1p) consists of several proline-rich sequences containing from 5 to 12 consecutive proline residues, and the FH2 domain (amino acids 1516 to 1616 in Bni1p) is characterized by a consensus sequence of ~100 amino acids.

Two-hybrid tests of protein-protein interactions demonstrated that Cdc42p can associate with Bni1p; the interaction was localized to amino acids 1 to 1214 of Bni1p (Table 1). The interaction of Cdc42p with Bni1p was specific for the activated form of Cdc42p: Cdc42p^{G12V}, a mutant form of Cdc42p that is expected to exist predominantly in the GTP-bound state, interacted with Bni1p, whereas Cdc42p^{D118A}, a mutant

form that is expected to remain in the GDP-bound or nucleotide-free state, did not (Table 1). Confirmation of the Cdc42p(GTP)-Bni1p interaction was obtained with a hemagglutinin A (HA) epitope-tagged fragment of Bni1p (amino acids 1 to 1214) purified from yeast cells and Cdc42p produced in *Escherichia coli*. GTP γ S-bound Cdc42p associated with the Bni1p fragment, but GDP-bound Cdc42p or nucleotide-free Cdc42p did not (Fig. 2A). We conclude that Bni1p may act as a target of GTP-bound Cdc42p during pheromone response.

To further explore the morphogenetic role of Bni1p, we examined changes in cell shape associated with overproduction of Bni1p or the NH₂-terminally truncated protein Bni1p(452–1953) (14). When grown on galactose, cells overexpressing full-length Bni1p from a *GAL1-BNI1* gene were nearly normal for growth and cell morphology (Fig. 1B). However, overexpression of Bni1p(452–1953) (from *GAL1-BNI1ΔN*) was toxic and caused de-

polarized growth resulting in large round cells. These aberrant cells displayed an unusual actin cytoskeleton that contained an abundance of actin cables and cortical actin patches (Fig. 1B). Although both *cdc42* mutations and several other mutations that affect the actin cytoskeleton produce similar depolarized morphologies, the accumulation of actin cables is an unusual phenotype (4, 15). To investigate the mechanism underlying the depolarization caused by *BNI1ΔN*, we screened for dosage suppressors of the induced lethality. The strongest suppressors proved to be *PFY1*, *TPM1*, and *TPM2* (16) (Fig. 2B), which encode the actin-binding proteins profilin (*PFY1*) and tropomyosin (*TPM1*, *TPM2*), respectively. Thus, the overexpression of *BNI1ΔN* may perturb cell polarization through aberrant interactions with profilin, tropomyosin, or both.

Profilin binds both to polyproline and to the proline-rich sequences of proteins implicated in actin assembly, such as human VASP and murine Mena (17). To determine if Bni1p associated with profilin, we examined two-hybrid interactions between Pfy1p and various regions of Bni1p. The profilin construct interacted both with yeast actin and with the FH1 domain of Bni1p (Table 2). Profilin may bind to the proline-rich sequences within the FH1 domain, because a mutant form of profilin, Pfy1p-3, which is defective for polyproline binding but normal for actin binding (18) (Table 2), failed to show a two-hybrid interaction with Bni1p (Table 2). We also detected interaction of a glutathione-S-transferase (GST)-profilin fusion protein purified from *Escherichia coli* and an HA epitope-tagged Bni1p fragment produced in yeast (Fig. 2C). Interaction with profilin may be required for normal Bni1p function, because deletion of the Bni1p FH1 domain yielded a mutant protein that failed to rescue the projection defect of *bni1* cells (19). Similarly, *Drosophila* profilin forms a com-

Table 1. Two-hybrid interactions between Cdc42p and Bni1p. Assays were done as described (28) with strain Y704; pJG4-5 was the vector control.

DNA-binding domain fusion	Activation-domain fusion	<i>lacZ</i> expression (Miller units)
Cdc42p	Vector	4.3 ± 0.2
Cdc42p	Bni1p(1–1953)	17.0 ± 0.2
Cdc42p	Bni1p(1–1214)	59.0 ± 2.0
Cdc42p	Bni1p(1215–1953)	4.1 ± 0.2
Cdc42p(G12V)	Vector	16.0 ± 1.0
Cdc42p(G12V)	Bni1p(1–1214)	122.0 ± 7.0
Cdc42p(D118A)	Vector	0.2 ± 0.1
Cdc42p(D118A)	Bni1p(1–1214)	0.1 ± 0.0

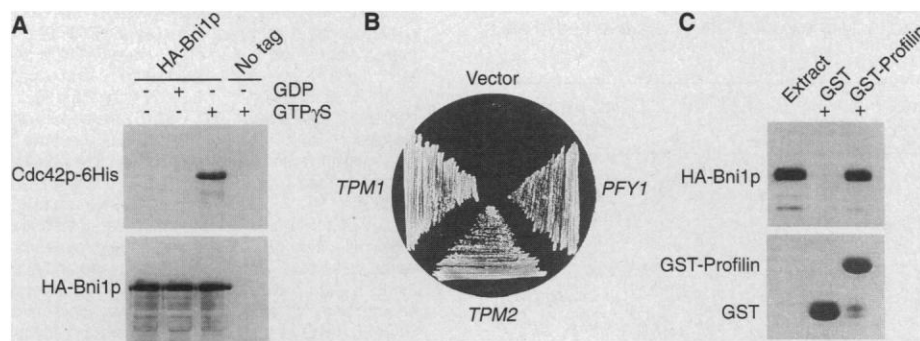


Fig. 2. Interaction of Bni1p with Cdc42p and the actin cytoskeleton. (A) Specific interaction between GTP-bound Cdc42p and Bni1p (27). Purified HA epitope-tagged Bni1p(1–1214) immobilized on Sepharose beads was incubated with purified Cdc42p-6His that had been loaded with GDP or GTP γ S or incubated without added nucleotide. Bound proteins were eluted and subjected to immunoblot analysis with antibodies to Cdc42p (upper panel) or the HA epitope (lower panel). (B) Increased dosage of the genes encoding profilin (*PFY1*) or tropomyosin (*TPM1* and *TPM2*) rescued the lethality caused by overexpression of *BNI1ΔN* (16). Cells containing *GAL1-BNI1ΔN* were transformed with a multicopy plasmid carrying *PFY1*, *TPM1*, or *TPM2*, or with the vector alone, and tested for colony formation on galactose medium. (C) Complex formation between Bni1p(1215–1953) and GST-profilin (30). GST-profilin or GST bound to glutathione-Sepharose beads was mixed with yeast extracts prepared from cells expressing an HA epitope-tagged Bni1p(1215–1953). Bound proteins were detected by immunoblot analysis with antibodies to HA (upper panel) and antibodies that recognize GST (lower panel).

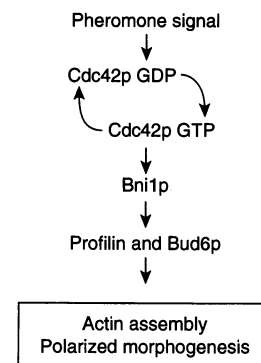


Fig. 3. Model for the role of Bni1p in reorganization of the actin cytoskeleton during the pheromone response.

plex with the formin encoded by *cappuccino* (20). The interaction between Bni1p and profilin is consistent with the possibility that Bni1p promotes actin polymerization because the complex of profilin with ATP-actin adds efficiently to the growing ends of actin filaments (21).

To identify additional proteins that associate with Bni1p, we developed the "catch and release" screen, which combines dosage suppression with the two-hybrid system (22). First, with a yeast two-hybrid library of activation-domain fusions, we selected for dosage suppressors of the lethality associated with a bait construct (DNA-binding domain fusion) containing *BNI1ΔN*. In a second step, we screened the suppressors for those that showed a positive two-hybrid interaction. This methodology led to multiple independent isolations of COOH-terminal fragments of Bud6p (Aip3p) (22), a protein that participates in bipolar budding and cellular morphogenesis and also shows a two-hybrid association with actin (9, 23). The Bud6p-Bni1p interaction involved the COOH-terminal domain of Bni1p (Table 2). We suspect that the Bud6p-Bni1p interaction is physiologically relevant, because *bud6* mutant cells share most of the phenotypes observed for *bni1* mutant cells during vegetative growth (9, 23). In addition, we found that *bud6* cells were defective in mating projection formation, although this defect was less severe than that of *bni1* mutants (24). Moreover, the localization of Bud6p overlaps

with that of Bni1p, occurring at the sites of surface growth during both budding (9, 23) and projection formation (Fig. 1D). These findings suggest that Bud6p and Bni1p are part of a complex that mediates reorganization of the actin cytoskeleton during polarized morphogenesis.

From another catch and release screen, based on a smaller but equally toxic *BNI1ΔN* fragment (22), we isolated multiple plasmids containing *ACT1* (actin) cDNAs, which interacted with the FH1 domain of Bni1p (Table 2). The interaction might reflect a complex in which endogenous yeast profilin bridges Bni1p and actin. In addition, a *bni1Δ::URA3* disruption mutation was synthetically lethal in combination with *act1-120* (25), a conditional actin mutation that produces morphological and budding defects similar to those of *bni1* cells. Thus, Bni1p can interact with actin, and *BNI1* is essential when yeast cells are compromised for actin function.

We suggest that Bni1p may occur as part of a complex that directs the assembly of actin filaments in response to Cdc42p signaling during polarized morphogenesis (Fig. 3). The NH₂-terminal portion of Bni1p interacts with Cdc42p, whereas the COOH-terminal portion interacts with profilin, Bud6p, and actin. Rho1p also binds to the NH₂-terminal portion of Bni1p (10), and we have observed the formation of Bni1p-Rho3p and Bni1p-Rho4p complexes (19). Thus, Bni1p may serve as a general target of yeast Rho proteins and thereby mediate a common

molecular function of these signaling molecules. A role in actin assembly may account for both the cytoskeletal and developmental functions of other members of the formin family (13, 20).

REFERENCES AND NOTES

1. J. Chenevert, *Mol. Biol. Cell* **5**, 1169 (1994); N. Valtz, M. Peter, I. Herskowitz, *J. Cell Biol.* **131**, 863 (1995); R. Dorer, P. M. Pryciak, L. H. Hartwell, *ibid.*, p. 845; J. Chant, *Curr. Opin. Cell Biol.* **8**, 557 (1996); I. Herskowitz, *Cell* **80**, 187 (1995).
2. T. Leeuw *et al.*, *Science* **270**, 1210 (1995).
3. L. M. Machesky and A. Hall, *Trends Cell Biol.* **6**, 304 (1996); A. J. Ridley, *Curr. Biol.* **6**, 1256 (1996).
4. D. I. Johnson and J. R. Pringle, *J. Cell Biol.* **111**, 143 (1990); A. E. M. Adams, D. I. Johnson, R. M. Longnecker, B. F. Sloat, J. R. Pringle, *ibid.*, p. 131; M. Ziman, J. M. O'Brien, L. A. Ouellette, W. R. Church, D. I. Johnson, *Mol. Cell Biol.* **11**, 3537 (1991); J. Chenevert, N. Valtz, I. Herskowitz, *Genetics* **136**, 1287 (1994); M.-N. Simon *et al.*, *Nature* **376**, 702 (1995).
5. B. J. Stevenson *et al.*, *Genes Dev.* **9**, 2949 (1995).
6. P. Madaule, R. Axel, A. M. Myers, *Proc. Natl. Acad. Sci. U.S.A.* **84**, 779 (1987); Y. Matsui and A. Toh-e, *Mol. Cell Biol.* **12**, 5690 (1992); H. Nonaka *et al.*, *EMBO J.* **14**, 5931 (1995); J. Drgonová *et al.*, *Science* **272**, 277 (1996); J. Imai, A. Toh-e, Y. Matsui, *Genetics* **142**, 359 (1996); H. Qadota *et al.*, *Science* **272**, 279 (1996).
7. M. Ziman *et al.*, *Mol. Biol. Cell* **4**, 1307 (1993).
8. R. Li, Y. Zheng, D. G. Drubin, *J. Cell Biol.* **128**, 599 (1995); D. G. Drubin and W. J. Nelson, *Cell* **84**, 335 (1996); T. Kirchhausen and F. S. Rosen, *Curr. Biol.* **6**, 676 (1996); N. Lamarche *et al.*, *Cell* **87**, 519 (1996).
9. R.-P. Jansen, C. Dowzer, C. Michaelis, M. Galova, K. Nasmyth, *Cell* **84**, 687 (1996); J. E. Zahner, H. A. Harkins, J. R. Pringle, *Mol. Cell Biol.* **16**, 1857 (1996); H. Fares, M. Longtine, J. R. Pringle, unpublished data.
10. H. Kohno *et al.*, *EMBO J.* **15**, 6060 (1996).
11. SY2625 (*MATa ura3-1 leu2-3,112 trp1-1 ade2-1 can1-100 sst1Δ mfa2Δ::FUS1-lacZ his3Δ::FUS1-HIS3*) or Y96 (*MATa ura3-1 leu2-3,112 trp1-1 ade2-1 can1-100 sst2::LEU2 lys2::GAL1-SST2 mfa2Δ::FUS1-lacZ his3Δ::FUS1-HIS3*) cells were mutagenized and screened for mating defects as described [N. Adames, K. Blundell, M. N. Ashby, C. Boone, *Science* **270**, 464 (1995)]. Analysis of genomic-DNA fragments that complemented the mating defects revealed that each screen identified a mutant defective in *BNI1* (9, 10); these were named Y37 (*bni1-10*, from SY2625) and Y270 (*bni1-11*, from Y96). Quantitative mating experiments [G. F. Sprague Jr., *Methods Enzymol.* **194**, 77 (1991)] indicated that SY2625 and Y37 mated with efficiencies of $30 \pm 5\%$ and $2.6 \pm 0.5\%$, respectively (averages and standard deviations from three independent experiments).
12. Y323 is an SY2625 (11) derivative carrying a chromosomal *bni1Δ::URA3* mutation, created with Xho I-Hind III-cut p321 (26). In the mating projection assay, cells were grown to mid-log phase and synthetic α -factor was added (500 ng/ml). After 3 hours, the morphology of 600 cells was scored. For SY2625, 99% of the cells were unbudded (*G*₁ arrested) and 68% had polarized projections. For Y323, 99% of the cells were unbudded but only 2% had formed polarized projections. In the *FUS1-lacZ* assay, cells were grown to mid-log phase and synthetic α -factor was added (100 ng/ml). After 1 hour, the cells were assayed for β -galactosidase activity as described [D. C. Hagen, G. McCaffrey, G. F. Sprague Jr., *Mol. Cell Biol.* **11**, 2952 (1991)]. We found that SY2625 and Y323 showed similar basal amounts of *FUS1-lacZ* expression and were induced 14 ± 1 - and 13 ± 2 -fold, respectively, by pheromone (averages and standard deviations of three independent assays).
13. D. C. Chan, A. Wynshaw-Boris, P. Leder, *Development* **121**, 3151 (1995); D. C. Chan, M. T. Bedford, P. Leder, *EMBO J.* **15**, 1045 (1996); D. H. Castrillon

Table 2. Two-hybrid interactions among profilin, actin, Bni1p, and Bud6p. Assays were done as described (28) with strains Y704 (for assays involving either DBD or AD profilin constructs and for vector controls) and Y523 (remaining assays). For a given DBD fusion, the AD vectors gave indistinguishable basal levels of *lexAop-lacZ* reporter expression; therefore, only one control assay is presented in each case.

DNA-binding domain fusion	Activation-domain fusion	<i>lacZ</i> expression (Miller units)
Pfy1p	Vector	0.2 ± 0.1
Pfy1p	Act1p	132.0 ± 5.0
Pfy1p	Bni1p(1-1953)	8.8 ± 1.0
Pfy1p	Bni1p(1-1214)	0.2 ± 0.0
Pfy1p	Bni1p(1227-1397)	64.0 ± 1.0
Pfy1p	Bni1p(1414-1953)	0.2 ± 0.1
Pfy1p	Bni1p(1647-1953)	0.5 ± 0.1
Bni1p(1227-1397)	Vector	0.4 ± 0.1
Bni1p(1227-1397)	Pfy1p	80.0 ± 2.0
Pfy1p-3	Vector	0.1 ± 0.0
Pfy1p-3	Act1p	127.0 ± 4.0
Pfy1p-3	Bni1p(1227-1397)	0.1 ± 0.0
Bni1p(1227-1397)	Vector	0.5 ± 0.1
Bni1p(1414-1953)	Vector	0.7 ± 0.2
Bni1p(1647-1953)	Vector	0.5 ± 0.0
Bni1p(1227-1397)	Bud6p(478-788)	0.5 ± 0.1
Bni1p(1414-1953)	Bud6p(478-788)	359.0 ± 54.0
Bni1p(1647-1953)	Bud6p(478-788)	296.0 ± 20.0
Bni1p(1227-1397)	Act1p	48.0 ± 0.3
Bni1p(1414-1953)	Act1p	0.4 ± 0.1
Bni1p(1647-1953)	Act1p	0.3 ± 0.1

- and S. A. Wasserman, *Development* **120**, 3367 (1994); S. Emmons *et al.*, *Genes Dev.* **9**, 2482 (1995); J. F. Marhoul and T. H. Adams, *Genetics* **139**, 537 (1995); S. D. Harris, L. Hamer, K. E. Sharpless, J. E. Hamer, *EMBO J.*, in press; J. Petersen, D. Weilguny, R. Egel, O. Nielsen, *Mol. Cell. Biol.* **15**, 3697 (1995); F. Chang, D. Drubin, P. Nurse, *J. Cell Biol.*, in press.
14. Cells of strains SY2625 (11) and Y323 (12) were grown to mid-log phase and synthetic α -factor was added (500 ng/ml). After 3 hours, the cells were stained for F-actin with rhodamine-phalloidin (Molecular Probes) as described [A. E. M. Adams and J. R. Pringle, *Methods Enzymol.* **194**, 729 (1991)]. Strains Y723 (*MATa ade8 Δ ::GAL1-BNI1 ura3-1 leu2-3,112 trp1-1 ade2-1 can1-100 mfa2 Δ ::FUS1-lacZ his3 Δ ::FUS1-HIS3*) and Y488 (*MATa ade8 Δ ::GAL1-BNI1 Δ N ura3-1 leu2-3,112 trp1-1 ade2-1 can1-100 mfa2 Δ ::FUS1-lacZ his3 Δ ::FUS1-HIS3*) were constructed from SY2585 [SST1 derivative of SY2625 (11)] by transformation and two-step gene replacement [R. Rothstein, *Methods Enzymol.* **194**, 281 (1991)] with Nru I-digested p849 and p414 (26), respectively. Cells of each strain were transferred from glucose to galactose medium, then stained with rhodamine-phalloidin after 12 hours.
 15. J. F. Amatruda, J. F. Cannon, K. Tatchell, C. Hug, J. A. Cooper, *Nature* **344**, 352 (1990); B. K. Haarer *et al.*, *J. Cell Biol.* **110**, 105 (1990); G. C. Johnston, A. Prendergast, R. A. Singer, *ibid.* **113**, 539 (1991); A. E. M. Adams, D. Botstein, D. G. Drubin, *Nature* **354**, 404 (1991); B. Drees, C. Brown, B. G. Barrell, A. Bretscher, *J. Cell Biol.* **128**, 383 (1995).
 16. To identify dosage suppressors of the lethality associated with overexpression of *BNI1 Δ N*, we transformed Y488 cells (14) with a yeast genomic library in the multicopy plasmid YEp24 [M. Carlson and D. Botstein, *Cell* **28**, 145 (1982)], then replica-plated the cells to galactose medium. Six plasmids that allowed Y488 to grow on galactose medium were isolated, and both ends of the inserts were sequenced. Each plasmid carried a genomic-DNA insert of 6 to 8 kb; two of these inserts contained *TPM1*, two contained *TPM2*, and two contained *PFY1*. In a screen that used a *GAL1*-driven cDNA library [H. Liu, J. Krizek, A. Bretscher, *Genetics* **132**, 665 (1992)], seven of the dosage suppressors were *TPM1*, two were *TPM2*, and two were *PFY1* (each cDNA encoded a full-length product).
 17. M. Reinhard *et al.*, *EMBO J.* **14**, 1583 (1995); F. B. Gertler, K. Niebuhr, M. Reinhard, J. Wehland, P. Soriano, *Cell* **87**, 227 (1996).
 18. B. K. Haarer, A. S. Petzold, S. S. Brown, *Mol. Cell. Biol.* **13**, 7864 (1993); D. A. Kaiser and T. D. Pollard, *J. Mol. Biol.* **256**, 89 (1996).
 19. M. Evangelista, K. Blundell, C. J. Chow, N. Adames, C. Boone, unpublished results.
 20. L. Manseau, J. Calley, H. Phan, *Development* **122**, 2109 (1996).
 21. H.-Q. Sun, K. Kwiatkowska, H. L. Yin, *Curr. Opin. Cell Biol.* **7**, 102 (1995).
 22. We refer to the combined dosage suppression-two-hybrid screen as a "catch and release" screen, because the library plasmids that are caught by the bait also release the host cells from the bait's lethal effect. This procedure is highly selective because it places an additional functional constraint on the product of the two-hybrid library plasmid. The first catch and release screen involved the overproduction of a fusion between the LexA DNA-binding domain and Bni1p(452-1953). Y595 (*ade8 Δ ::GAL1-lexABNI1 Δ N ura3-1::URA3 lexAop-lacZ leu2-3,112 trp1-1 ade2-1 can1-100*) was created from W303-1A (27) in a two-step gene replacement (14) with p529 (26) and integration of pSH18-34 Δ spe (26). Y595 cells were transformed with a two-hybrid library containing yeast genomic DNA fragments fused to the activation domain of pGAD-C (28). The library plasmids that both rescued the lethality of Y595 cells on galactose medium and led to expression of the *lexAop-lacZ* reporter (observed by replica-plating to X-Gal plates) were recovered for sequence analysis. Approximately 2×10^6 potential transformants were processed, and 17 positive clones were isolated. All 17 clones encoded either the 503 or 311 COOH-terminal amino acids of Bud6p (Aip3p) (23). The COOH-terminal domain of Bud6p also shows a two-hybrid interaction with actin (23). A second screen used a fusion of the LexA DNA-binding domain to Bni1p(1215-1953), Y777 (*ade8 Δ ::GAL1-lexABNI1 Δ N2 ura3-1::URA3 lexAop-lacZ leu2-3,112 trp1-1 ade2-1 can1-100*) was created as described for strain Y595 but with plasmid p997 (26). Y777 cells were transformed with a yeast cDNA two-hybrid library of activation domain fusions in pACT (28), and positive clones were identified as described above. From 2×10^6 potential transformants, 11 positive plasmids were isolated, all of which contained full-length *ACT1* cDNAs.
 23. D. C. Amberg, J. E. Zahner, J. W. Mulholland, J. R. Pringle, D. Botstein, *Mol. Biol. Cell.*, in press.
 24. Y773 is an SY2625 (11) derivative carrying a *bud6 Δ ::URA3* mutation, created with Hind III-Sst I-cut p1055 (26). Upon exposure to pheromone in a projection assay (12), 99% of the Y773 cells were unbudded, and 17% of these cells also formed a polarized mating projection. Under similar conditions, 68% of wild-type cells and 2% of *bni1 Δ ::URA3* cells formed polarized projections (12).
 25. Like *bni1* and *bud6* mutant cells (9, 10, 23), *act1-120* cells are defective for bipolar budding and develop a round cell shape with wide bud necks [D. G. Drubin, H. D. Jones, K. F. Wertman, *Mol. Biol. Cell.* **4**, 1277 (1993); S. Yang, K. Ayscough, D. G. Drubin, *J. Cell Biol.* **137**, 111 (1997)]. DBY5551 (*MATa/MAT α act1-120::HIS3/ACT1 tub2/TUB2 his3-200/his3-200 leu2/leu2 ura3/ura3 ade2/ADE2 can1/CAN1 cry1/CRY1 ade4/ADE4*) [K. F. Wertman, D. G. Drubin, D. Botstein, *Genetics* **132**, 337 (1992)] was transformed with Hind III-Xho I-cut p321 (26) to create strain Y821, heterozygous for a *bni1 Δ ::URA3* mutation. Y821 was sporulated, and tetrads were dissected on rich medium at 23°C. From 86 tetrads, 79 of the viable spore progeny were *bni1 Δ ::URA3 ACT1*, 79 were *BNI1 act1-120::HIS3*, and 93 were *BNI1 ACT1*. The 93 presumed *bni1 Δ ::URA3 act1-120::HIS3* double mutants either failed to germinate or formed microcolonies too small to characterize further.
 26. Plasmid p182 carries an 8.5-kb fragment that contains *BNI1* isolated from a yeast genomic library [C. Boone, K. L. Clark, G. F. Sprague Jr., *Nucleic Acids Res.* **20**, 4661 (1992)] in vector pRS316 [R. S. Sikorski and P. Hieter, *Genetics* **122**, 19 (1989)] by complementation of the *bni1-11* mating defect. In p182, the *BNI1* open reading frame is directed toward the Not I site of the pRS316 polylinker, and the entire *BNI1* genomic insert can be removed from the vector as an 8.5-kb Bam HI to Not I fragment. To create plasmid p321, containing a *bni1 Δ ::URA3* allele, we cloned a 2.4-kb Xho I-Hind III fragment from p182 into KS+ (Stratagene), and inserted a *URA3* fragment into the Bgl II sites within *BNI1*; this deleted the *BNI1* sequence encoding amino acids 1229 to 1415 and left the downstream *BNI1* sequence out of frame. pY39tet1 is a multicopy plasmid that contains full-length Bni1p with a COOH-terminal tag composed of four tandem copies of the HA epitope (9). To create plasmid p532, carrying *BNI1* with a Bam HI site just upstream of its ATG codon, we amplified a 1.3-kb fragment of *BNI1* by the polymerase chain reaction with primers (5'-TGGATCCGCGAAATGTTGAAGAATCTAGGCTCC-3' and 5'-AGCGGC-CGCTTAAAGTGGCCATTTCTTGTAGCCAGTTTCGTAGAAAGTAAACC-3') that incorporated Bam HI and Msc I sites (underlined), and the product was ligated into p182 cut with Bam HI and Msc I. p527 is a pRS316-based vector that carries the *GAL1* promoter regulating a sequence encoding three copies of the HA epitope [P. A. Kolodziej and R. A. Young, *Methods Enzymol.* **194**, 508 (1991)] followed by Bam HI and Not I cloning sites. p827 contains the 3.6-kb Bam HI to Eco 47III fragment of p532, encoding Bni1p(1-1214), ligated in frame with the HA epitope sequences of p527. p828 is an expression vector similar to p827 except that it lacks the HA epitope sequence. p1025 contains the 3.9-kb Eco 47III to Not I fragment of p182 [encoding Bni1p(1215-1953)], ligated in frame with the HA epitope sequence of p527. p907 contains a Bam HI to Not I fragment, containing a full-length profilin cDNA (16), ligated in frame with the GST sequences of pGEX-3X (Pharmacia). To create p1055, carrying a *bud6::URA3* allele, we ligated a 2.2-kb Hind III-Sst I fragment of *BUD6* (*AIP3*) (23) into KS+ and inserted a *URA3* fragment at the Sna BI site, thus disrupting *BUD6* after its ninth codon. For integration of *GAL1-BNI1* and *GAL1-BNI1 Δ N* at the *ADE8* locus, the Bam HI to Not I fragment from p532 (encoding full-length Bni1p) and the Msc I to Not I fragment from p182 [encoding Bni1p(452-1953)] were ligated downstream of the *GAL1* promoter in p407, creating p849 and p414, respectively. p407 is a Ylplac211-based vector [R. D. Gietz and A. Sugino, *Gene* **74**, 527 (1988)] that contains the *GAL1* promoter inserted within an *ADE8* fragment. Digestion of p407-derived plasmids with Nru I (or Msc I) targeted integration to *ADE8*. For integration of *GAL1-lexABNI1 Δ N* at *ADE8*, a fragment encoding the LexA DBD was introduced upstream of *BNI1 Δ N* in p414, creating p529. p850 contains the *BNI1 Δ N2* Eco47 III-Not I fragment from p182 [encoding Bni1p(1215-1953)] ligated downstream of the *GAL1* promoter in p407. For integration of *GAL1-lexABNI1 Δ N2* at *ADE8*, a fragment encoding the LexA DBD was introduced upstream of *BNI1 Δ N2* in p850, creating p997. pSH18-34 Δ spe is an integrating plasmid that carries *URA3* and a *lexAop-lacZ* reporter. pSH18-34 Δ spe was targeted for integration at *URA3* by digestion with *Apa* I.
 27. W303-1A (*MATa ura3-1 leu2-3,112 his3-11,15 trp1-1 ade2-1 can1-100*) cells carrying p827 or p828 (26) were grown to mid-log phase in raffinose medium, then galactose was added. After 1 hour, extracts were prepared as described [M. Peter, A. M. Neiman, H.-O. Park, M. van Lohuizen, I. Herskowitz, *EMBO J.* **15**, 7046 (1996)]. HA-tagged Bni1p(1-1214) was purified with monoclonal antibody HA.11 (29) covalently coupled to protein G-Sepharose. Full-length Cdc42p was expressed in *E. coli* as a protein tagged with six consecutive histidine residues (6His) using pTrcHis (Invitrogen), then purified on a column containing iminodiacetic acid immobilized on Sepharose-6B (Sigma) and coupled to Co²⁺. The purified Cdc42p was incubated without added nucleotide or loaded with either GDP or GTP γ S as described [H. O. Park, J. Chant, I. Herskowitz, *Nature* **365**, 269 (1993)], then incubated for 1 hour at 4°C with the immobilized HA-Bni1p(1-1214) in 200 μ l of buffer B [10 mM tris-HCl (pH 7.5), 85 mM NaCl, 6 mM MgCl₂, 10% glycerol, 0.6 mM GTP γ S or 0.6 mM GDP]. After four washes with buffer TMT [10 mM tris-HCl (pH 7.5), 10 mM MgCl₂, 1 mM dithiothreitol, 0.1% Triton X-100], the bound proteins were eluted by boiling in SDS-polyacrylamide gel electrophoresis sample buffer and subjected to immunoblot analysis with antibodies to Cdc42p [M. Peter *et al.*, *EMBO J.* **15**, 7046 (1996)] or HA.11 as described [M. Peter, A. Gartner, J. Horecka, G. Ammerer, I. Herskowitz, *Cell* **73**, 747 (1993)].
 28. Two-hybrid experiments [E. M. Phizicky and S. Fields, *Microbiol. Rev.* **59**, 94 (1995)] were performed with strain Y704 (*MATa lexAop-LEU2 lexAop-lacZ sst1 Δ his3 trp1 ura3-52 leu2*) or Y523 (*MATa lexAop-lacZ leu2 his3 trp1 ade2 lys2 gal80 GAL4*). These strains were transformed with both a LexA DNA-binding domain (DBD) plasmid and a transcriptional-activation domain (AD) plasmid, then assayed for expression of *lexAop-lacZ*. Cells were grown to mid-log phase in medium containing 2% raffinose, galactose was added to a concentration of 2%, and growth was continued for 4 hours before assaying for β -galactosidase activity (12). Each value represents the average and standard deviation for three independent cultures. The DBD plasmids were pEG202 [J. Gyuris, E. Golemis, H. Chertkov, R. Brent, *Cell* **75**, 791 (1993)] derivatives expressing DBD fusion proteins. The AD plasmids were pJG4-5 [J. Gyuris *et al.*, *ibid.*, p. 791], pGAD-C [P. James, J. Halladay, E. A. Craig, *Genetics* **144**, 1425 (1996)], pACT [T. Durfee *et al.*, *Genes Dev.* **7**, 555 (1993)], and derivatives expressing AD fusion proteins. DBD-Cdc42p fusions (5) all incorporate the C188S substitution, which prevents prenylation. Other DBD plasmids used were

A General Model for the Origin of Allometric Scaling Laws in Biology

Geoffrey B. West, James H. Brown,* Brian J. Enquist

Allometric scaling relations, including the 3/4 power law for metabolic rates, are characteristic of all organisms and are here derived from a general model that describes how essential materials are transported through space-filling fractal networks of branching tubes. The model assumes that the energy dissipated is minimized and that the terminal tubes do not vary with body size. It provides a complete analysis of scaling relations for mammalian circulatory systems that are in agreement with data. More generally, the model predicts structural and functional properties of vertebrate cardiovascular and respiratory systems, plant vascular systems, insect tracheal tubes, and other distribution networks.

Biological diversity is largely a matter of body size, which varies over 21 orders of magnitude (1). Size affects rates of all biological structures and processes from cellular metabolism to population dynamics (2, 3). The dependence of a biological variable Y on body mass M is typically characterized by an allometric scaling law of the form

$$Y = Y_0 M^b \quad (1)$$

where b is the scaling exponent and Y_0 a constant that is characteristic of the kind of organism. If, as originally thought, these relations reflect geometric constraints, then b should be a simple multiple of one-third. However, most biological phenomena scale as quarter rather than third powers of body mass (2–4): For example, metabolic rates B of entire organisms scale as $M^{3/4}$; rates of cellular metabolism, heartbeat, and maximal population growth scale as $M^{-1/4}$; and times of blood circulation, embryonic growth and development, and life-span scale as $M^{1/4}$. Sizes of biological structures scale similarly: For example, the cross-sectional areas of mammalian aortas and of tree trunks scale as $M^{3/4}$. No general theory explains the origin of these laws. Current hypotheses, such as resistance to elastic buckling in terrestrial organisms (5) or diffusion of materials across hydrodynamic boundary layers in aquatic organisms (6), cannot explain why so many biological processes in nearly all kinds of animals (2, 3), plants (7), and microbes (8) exhibit quarter-power scaling.

We propose that a common mechanism

underlies these laws: Living things are sustained by the transport of materials through linear networks that branch to supply all parts of the organism. We develop a quantitative model that explains the origin and ubiquity of quarter-power scaling; it predicts the essential features of transport systems, such as mammalian blood vessels and bronchial trees, plant vascular systems, and insect tracheal tubes. It is based on three unifying principles or assumptions: First, in order for the network to supply the entire volume of the organism, a space-filling fractal-like branching pattern (9) is required. Second, the final branch of the network (such as the capillary in the circulatory system) is a size-invariant unit (2). And third, the energy required to distribute resources is minimized (10); this final restriction is basically equivalent to minimizing the total hydrodynamic resistance of the system. Scaling laws arise from the interplay between physical and geometric constraints implicit in these three principles. The model presented here should be viewed as an idealized representation in that we ignore complications such as tapering of vessels, turbulence, and nonlinear effects. These play only a minor role in determining the dynamics of the entire network and could be incorporated in more detailed analyses of specific systems.

Most distribution systems can be described by a branching network in which the sizes of tubes regularly decrease (Fig. 1). One version is exhibited by vertebrate circulatory and respiratory systems, another by the "vessel-bundle" structure of multiple parallel tubes, characteristic of plant vascular systems (11). Biological networks vary in the properties of the tube (elastic to rigid), the fluid transported (liquid to gas), and the nature of the pump (a pulsatile compression pump in the cardiovascular system, a pulsatile bellows pump in the respiratory system, diffusion in insect

p888, which contains a Bam HI to Not I fragment encoding a full-length profilin cDNA (16); p989, which encodes a mutant form of profilin, Pfy1p-3, lacking the last three amino acids (18); p890, which contains the Bgl II to Stu I fragment from p182 (26), encoding Bni1p(1227–1397); p813, which contains the Bgl II to Not I fragment from p182, encoding Bni1p(1647–1953). The pJG4-5–derived plasmids were p561, which contains the Bam HI to Not I fragment from p532 (26), encoding Bni1p(1–1953); p717, which contains the Bam HI to Eco47 III fragment from p532, encoding Bni1p(1–1214); p558, which contains the Eco 47III to Not I fragment from p182, encoding Bni1p(1215–1953); p913, which contains the Bgl II to Stu I fragment from p182, encoding Bni1p(1227–1397); p929, which contains the Bgl II to Not I fragment from p182, encoding Bni1p(1414–1953); p952, which contains the Hpa I to Not I fragment from p182, encoding Bni1p(1647–1953); and p887, which contains the Bam HI to Not I fragment encoding a full-length profilin cDNA (16). The pACT-derived plasmid was p1124, encoding full-length Act1p as isolated in a catch and release screen (22). The pGAD-C–derived plasmid was p688, encoding the COOH-terminal 311 amino acids (478–788) of Bud6p, as isolated in a catch and release screen (22).

29. For localization of Bni1p, SY2625 (11) cells carrying a multicopy plasmid encoding either HA-tagged Bni1p [pY39tet1 (9)] or nontagged Bni1p were induced to form mating projections (12). HA-Bni1p was localized by immunofluorescence with monoclonal antibody HA.11 (Berkeley Antibody Company) as described [J. R. Pringle, A. E. M. Adams, D. G. Drubin, B. K. Haarer, *Methods Enzymol.* **194**, 565 (1991)]. For localization of Bud6p, SY2625 cells expressing GFP-Bud6p (23) or containing the control plasmid pRS316 (26) were induced to form mating projections (12), then observed by fluorescence microscopy with the use of a fluorescein isothiocyanate filter set.
30. Yeast cells of strain B5459 (*MATa pep4::HIS3 prb1Δ1-6R ura3 trp1 lys2 leu2 his3Δ200 can1*) carrying p1025 (26) were grown to mid-log phase in raffinose medium, and galactose was added to induce the production of HA-tagged Bni1p(1215–1953). After 1 hour, extracts were prepared by grinding cells with glass beads in lysis buffer [0.6 M sorbitol, bovine serum albumin (1%), 140 mM NaCl, 5 mM EDTA, 50 mM Tris-HCl (pH 7.6), 0.06% Triton X-100, 2 mM phenylmethylsulfonyl fluoride, aprotinin (10 μg/ml)] as described (2). *Escherichia coli* strain BL 21 (Novogen) was transformed with pGEX-3X (Pharmacia) or p907 (26) and induced for expression of GST or GST-profilin, respectively. GST proteins were purified on glutathione-Sepharose (Pharmacia) and washed twice with phosphate-buffered saline (PBS) [140 mM NaCl, 2.7 mM KCl, 10 mM Na₂HPO₄, 1.8 mM KH₂PO₄ (pH 7.3)]. Glutathione-Sepharose beads with GST or GST-profilin bound were then added to the yeast extract containing HA-Bni1p(1215–1953) and incubated on ice. After 45 min, the beads were collected and washed twice with PBS. The GST proteins and associated proteins were eluted with glutathione [10 mM glutathione, 50 mM Tris-HCl (pH 8.0)] and subjected to immunoblot analysis with antibodies to GST (Pharmacia) or the HA epitope (29) as described (27).
31. We thank D. Amberg, B. Andrews, R. Brent, R. Dorer, S. J. Elledge, S. Givan, B. K. Haarer, J. Horecka, P. James, I. Sadowski, M. Tyers, and J. Zahner for plasmids and yeast strains; B. Brandhorst, J. Brown, N. Davis, S. Kim, B. Nelson, and I. Pot for comments on the manuscript; and G. Poje and I. Pot for assistance with experiments. Supported by grants to C.B. from the Natural Sciences and Engineering Research Council of Canada and the National Cancer Institute of Canada; by a grant from the Swiss National Science Foundation to M.P.; and by NIH grant GM31006 to J.R.P.

2 December 1996; accepted 10 February 1997

G. B. West, Theoretical Division, T-8, Mail Stop B285, Los Alamos National Laboratory, Los Alamos, NM 87545, and The Santa Fe Institute, 1399 Hyde Park Road, Santa Fe, NM 87501, USA.
J. H. Brown and B. J. Enquist, Department of Biology, University of New Mexico, Albuquerque, NM 87131, and The Santa Fe Institute, 1399 Hyde Park Road, Santa Fe, NM 87501, USA.

*To whom correspondence should be addressed. E-mail: jhbrown@unm.edu